Photometric Redshifts in Hubble Deep Field South

D.L. Clements

Dept. Physics and Astronomy, Cardiff university, PO Box 913, Cardiff, CF22 3YB, UK

Abstract. We apply both a traditional 'dropout' approach and a photometric redshift estimation technique to the Hubble Deep Field South data. We give a list of dropout selected z∼3 objects, and show their images. We then discuss our photometric redshift estimation technique, demonstrate both its effectiveness and the role played by near-IR data, and then apply it to HDF-S to obtain an estimated redshift distribution.

1. Introduction

Techniques for photometric redshift estimation have advanced considerably since the original Hubble Deep Field (North) (HDF-N) observations (Williams et al., 1996). Initial techniques for identifying candidate high redshift objects in HDF-N were inspired by the famous 'dropout' techniques originally developed by Steidel et al. (see paper in these proceedings, and references therein). These have proved highly successful, and have identified several galaxies at z>5 (eg. Weymann et al., 1998, Spinrad et al., 1998). Since then, more sophisticated approaches to redshift estimation have been developed (eg. Fernandez-Soto et al., 1998) which aim to determine a redshift estimate rather than just select objects likely to have a redshift in some broad range (eg. 2.5<z<3.5 for F300W dropouts in one of the Hubble Deep Fields). The advent of the Hubble Deep Field South (HDF-S) observations (Williams et al., 1999), which include not only the optical WFPC-2 observations similar to HDF-N, but also STIS UV/optical observations and NICMOS near-IR observations, allow us to apply all these techniques to new fields and new wavelengths. We also benefit from the extensive followup programme on HDF-N for validating and training the various methods. The present paper describes the application of both traditional 'dropout' techniques, to select candidate high redshift objects in HDF-S, and a 'template matching' photometric redshift estimation scheme for determining redshift estimates for all the detected objects.

2. Selecting High Redshift Candidates by the 'Dropout' Method

The simple 'dropout' technique relies on the passage of the 912Å Lyman-limit discontinuity through broad-band imaging filters as a function of redshift. At higher redshifts, the suppression of light between 1216Å and 912Å in the emitted frame by the Lyα forest becomes significant, so that 1216Å becomes the breakpoint in the spectra (Spinrad et al., 1998). This allows one to select candi-

date high redshift objects by their colours in broad band filters. Typically, the objects are chosen by their absence in a blue filter, and their relatively flat SEDs at redder wavelengths. The classic application of this approach was by Steidel et al. (1995) who used three filters, U, G and R, to select candidate z$\sim$3 objects by their absence in the U filter. Similarly, 2.5<z<3.5 objects were selected in HDF-N by their absence in the F300W filter (eg. Clements & Couch, 1996). The technique can also be applied to longer wavelength filters for the selection of still higher redshift objects. For example, the z=5.34 galaxy discussed in Spinrad et al. 1998 was discovered as a V-band (F606W) dropout in the HDF-N images. The advent of HDF-S, which has coverage extending to 2.2μm in the NICMOS field, thus offers the possibility of uncovering galaxies with redshifts >>10 if we operate at the longest wavelengths.

Much has been learned about high redshift galaxies from experience with HDF-N, so we can tune the selection criteria for HDF-S for greater effectiveness. Consideration of the colour-colour plots in Dickinson et al. (1998) suggests that the following criteria will efficiently select candidate high redshift objects that drop out from a given filter a (all magnitudes referred to are in the AB system):

1. The colour between filter a and the next reddest filter b >1.5
2. The object should have been detected with at least 10σ significance in filter a if the colour $a - b = 1.5$
3. There is no more than 1 magnitude difference between the flux in any adjacent filters redder than b

However, at redder wavelengths, there are increasing possibilities for foreground interlopers to turn up in these simple colour selections. Specific problems include the 4000Å–break in evolved galaxies, and the unusual Very Red Objects. Both of these can masquerade as 'dropouts' especially at high redshift. Additional observations in the near-IR for the WFPC-2 field, or optical for the NICMOS field would help to reduce this contamination.

We apply these criteria to catalogs of HDF-S galaxies extracted from the images using SExtractor (Bertin & Arnouts, 1996). We uncover 15 candidate z$\sim$3 objects (F300W dropouts), 1 z$\sim$4 object (F450W dropout), and 16 candidate z$\sim$5 (F606W dropouts) in the 4.7 sq. arcmin. WFPC-2 field. Further examination leads us to believe that 4 of the F300W objects are in fact nearby interlopers, and that there is significant foreground contamination of the F606W dropout list. In the NICMOS field we find 4 candidate z$\sim$6 ('optical' dropouts — absent from the STIS open-band optical image but present at F110W) one candidate z$\sim$8 object (F110W dropout) and no candidate z$\sim$12 objects (F160W dropouts). One of the 'optical' dropouts is the VRO suspected to lie at z>1.7 discussed by Treu et al. (1998, 1999), and we suspect other VROs contaminate the NICMOS list.

Images for the F300W dropouts are shown in Fig. 1 and basic parameters given in Table 1. As can be seen, many of these objects appear to have quite disturbed morphologies, similar to the F300W dropouts discovered in HDF-N. Whether this is a true reflection of the underlying galaxy morphology or a result of these observations lying in the rest-frame far-UV is at this stage unclear. For more information on this work, and for a full catalog of high redshift candidates, see Clements et al. (1999).

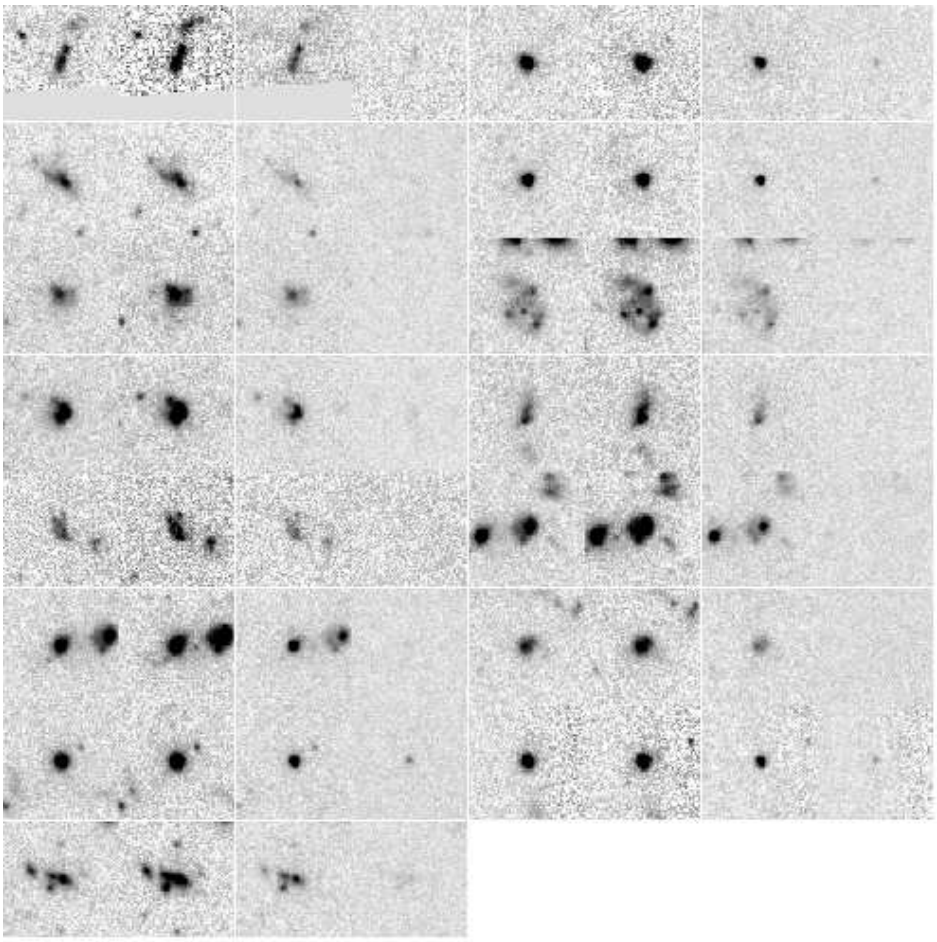

Figure 1. Images of F300W dropouts. Images are shown in groups of four horizontally, showing F814W, F606W, f450W and F300W images from left to right. Objects are shown in the same order as in Table 1, starting in the top left, then left to right, and then working down the page. Images are 4 arcseconds on a side. North is up and East is to the right.

WFPC2 Cat. No.	RA(J2000)	Dec(J2000)	F814	F606	F450	F300
z$\sim$ 3 F300 Dropout Candidates						
38	22 32 53.98	-60 34 20.53	24.76±0.08	24.96±0.04	25.08±0.13	26.60±0.6
149[1]	22 32 53.33	-60 34 13.69	22.83±0.02	23.21±0.01	23.88±0.04	26.14±0.26
257	22 32 59.91	-60 34 05.02	24.14±0.02	24.90±0.02	25.29±0.06	27.01±0.47
760[1]	22 32 58.10	-60 33 37.08	23.13±0.01	23.60±0.01	24.29±0.03	26.28±0.29
877	22 33 04.89	-60 33 29.48	24.31±0.03	24.43±0.01	24.68±0.04	>27.8
880	22 32 50.64	-60 33 28.84	24.45±0.03	24.72±0.02	25.07±0.05	>27.8
895	22 33 03.19	-60 33 28.77	23.34±0.02	23.68±0.01	24.02±0.03	26.20±0.25
1158	22 33 03.87	-60 33 12.89	24.56±0.04	24.77±0.02	25.15±0.07	>26.6
1562	22 32 57.22	-60 32 41.50	24.55±0.04	24.78±0.02	25.03±0.07	27.00±0.69
1745	22 32 49.00	-60 32 26.85	23.44±0.02	23.61±0.01	24.14±0.03	>27.8
1748	22 32 49.22	-60 32 27.09	23.00±0.01	23.20±0.01	23.68±0.03	>26.9
1816	22 32 47.62	-60 32 20.61	24.43±0.03	24.84±0.02	25.26±0.06	>26.9
1847[1]	22 32 47.76	-60 32 17.59	22.72±0.01	23.15±0.01	23.72±0.03	25.71±0.16
1934[1]	22 32 46.51	-60 32 08.38	22.97±0.02	23.40±0.01	24.07±0.04	26.61±0.41
1951	22 32 48.87	-60 32 06.71	24.11±0.02	24.32±0.01	24.54±0.04	26.07±0.21

Table 1. Details of drop out galaxies
Limits are 3σ upper limits. [1] indicates likely low redshift interloper.

3. Photometric Redshift Techniques

A more recent approach to multicolour surveys such as HDF-S is to obtain a full photometric redshift solution. There are a number of approaches to this, as can be seen from many of the other papers in these proceedings. The approach adopted here, similar to that of Fernandez-Soto et al. (1998), is to match a template spectral energy distribution (SED) at a given redshift to the photometric data for a galaxy. The likelihood that a galaxy is at the assumed redshift can then be calculated:

$$ln(L) = \sum_{filters} -\left(\frac{F_{obs} - F_{mod}(z,n)}{E_{obs}}\right)^2$$

where F_{obs} is the observed flux in a given filter, $F_{mod}(z)$ is the flux predicted for this filter from the template SED given a redshift z and a normalisation n, and E_{obs} is the error in the observed flux. This calculation of likelihood makes the implicit assumption that the flux errors are Gaussian. This likelihood is then maximised to find the most likely redshift for the galaxy given the assumed template and certain astrophysical constraints for the galaxy's properties. A selection of templates must be used. In the present work we use six templates: elliptical, Sab, Scd and Irregular types with SEDs taken from Coleman, Wu & Weedman (1980) and extrapolated to the infrared with GISSEL model SEDs (Bruzual & Charlot, 1996), and two starburst types with differing extinctions taken from Kinney et al. (1996), again with IR extrapolation using GISSEL models. We account for the effects of the Lyα forest absorption using a parametrisation based on Madau (1995).

The effectiveness of this method can be tested using the HDF-N data for objects which have spectroscopic redshifts. 108 such objects appear in the compendium of Fernandez-Soto et al. (1998), and are used as a test data set. The compendium includes infrared fluxes in J, H and K for the objects and these are particularly useful for constraining redshifts. Figure 2 shows the effectiveness of our photometric redshift technique both with and without the near-IR observations. A number of improvements to the method are still possible, for example we are developing a better treatment for the Lyman-forest absorption.

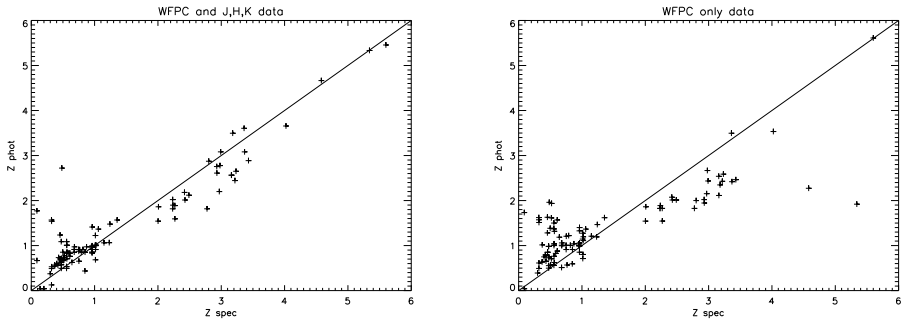

Figure 2. Test of photometric redshift estimation
Left, with near-IR data, right with only WFPC-2 data. 108 galaxies from Fernandez-Soto et al. (1998) with spectroscopic redshifts and fluxes at F300W, F450W, F606W, F814W, J, H and K are used for this test.

We thus expect the estimations to become more accurate. However, the method can clearly already be used as a fairly reliable selector of candidate high redshift objects.

We then apply our photometric redshift technique to the current catalogue of objects in HDF-S (Williams et al., 1999). At present we only include the WFPC-2 data, which will limit the accuracy of our redshift estimates. IR will soon be added to the catalogue. In Figure 3 we present the redshifts distribution for HDF-S derived from our photometric redshift estimation.

Acknowledgments.

References

Bertin, E., Arnouts, S., 1996, A&AS, 117, 393

Bruzual, G., & Charlot, S., 1996, in proceedings of IAU Symposium 171 'New Light on Galaxy Evolution', eds. Bender, R., & Davies, R.L., pub. Kluwer

Clements, D.L. & Couch, W.J., 1996, MNRAS, 280, L43

Clements, D.L., et al., 1999, MNRAS, in press, astro-ph/9906411

Coleman et al., 1980, ApJS, 43, 393

Dickinson, M., 1998, in proceedings of the STScI symposium 'The Hubble Deep Field', ed. Livio, M., Fall, S.M., Madau, P., in press, astro-ph/9802064

Fernandez-Soto, A., et al., 1998, ApJ., submitted, astro-ph/9809126

Kinney, A.L., et al., 1996, ApJ., 467, 38

Madau, P., 1995, ApJ., 441, 18

Spinrad, H., et al., 1998, AJ, 116, 2617

Steidel, C.C., et al., 1995, AJ, 110, 2519

Treu et al., 1998, A&A, 340, L10

Treu et al., 1999, A&A, in press

Weymann, R.J., et al., 1998, astro-ph/9807208

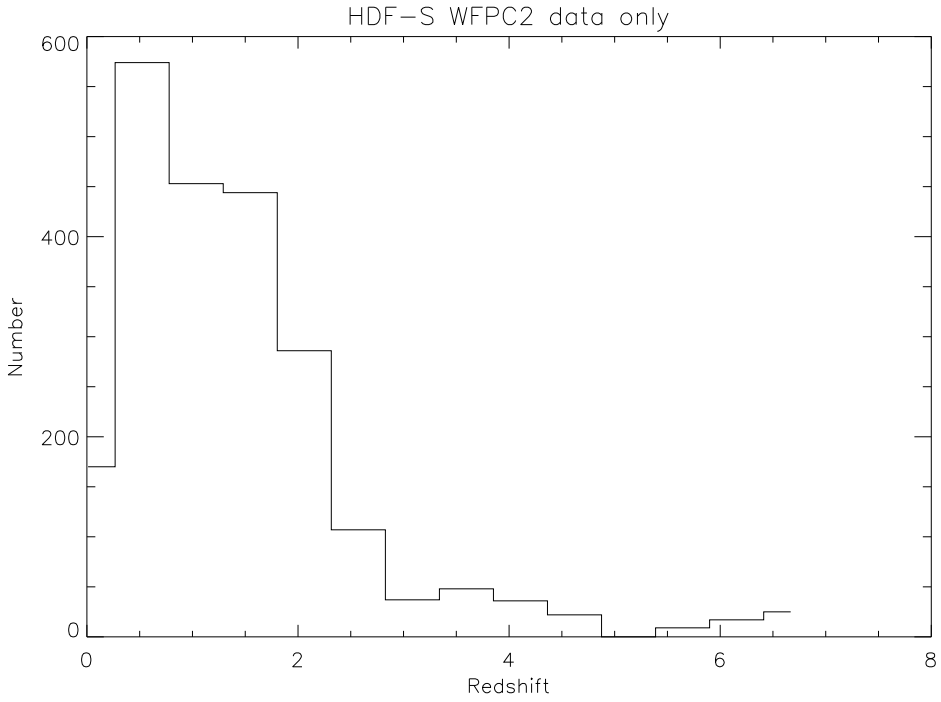

Figure 3. Photometricly estimated redshift distribution for HDF-S

Williams, R., et al., 1996, AJ, 112, 1335
Williams, R., et al., 1999, AJ, in press